

Deep Crustal Heating by Neutrinos from the Surface of Accreting Neutron Stars

F. J. Fattoyev,^{1,*} Edward F. Brown,^{2,†} Andrew Cumming,^{3,‡} Alex Deibel,^{4,§} C. J. Horowitz,^{1,¶} Bao-An Li,^{5,**} and Zidu Lin^{1,††}

¹*Center for Exploration of Energy and Matter and Department of Physics, Indiana University, Bloomington, IN 47405, USA*

²*Department of Physics and Astronomy, Michigan State University, 567 Wilson Rd, East Lansing, MI 48864, USA*

³*Department of Physics and McGill Space Institute, McGill University, 3600 rue University, Montreal QC, Canada H3A 2T8*

⁴*Department of Astronomy, Indiana University, Bloomington, IN 47405, USA*

⁵*Department of Physics and Astronomy, Texas A&M University-Commerce, Commerce, TX 75429, USA*

(Dated: July 2, 2018)

We present a new mechanism for deep crustal heating in accreting neutron stars. Charged pions (π^+) are produced in nuclear collisions on the neutron star surface during active accretion and upon decay they provide a flux of neutrinos into the neutron star crust. For massive and/or compact neutron stars, neutrinos deposit $\approx 1\text{--}2\text{ MeV}$ of heat per accreted nucleon into the inner crust. The strength of neutrino heating is comparable to the previously known sources of deep crustal heating, such as from pycnonuclear fusion reactions, and is relevant for studies of cooling neutron stars. We model the thermal evolution of a transient neutron star in a low-mass X-ray binary, and in the particular case of the neutron star MXB 1659-29 we show that additional deep crustal heating requires a higher thermal conductivity for the neutron star inner crust. A better knowledge of pion production cross sections near threshold would improve the accuracy of our predictions.

PACS numbers: 25.40.Qa, 25.40.Sc, 26.60.Gj, 26.60.Kp, 97.60.Jd

I. INTRODUCTION

Neutron stars in X-ray binaries accrete matter from their companion stars. As matter is accreted by the star, the crust is continually compressed and undergoes a series of non-equilibrium nuclear reactions such as electron captures, neutron emissions and pycnonuclear fusion reactions that release $\approx 1\text{--}2\text{ MeV}$ per accreted nucleon [1–5]. Energy release mainly occurs in the inner crust at mass densities of about $10^{12}\text{--}10^{13}\text{ g cm}^{-3}$ and is referred to as deep crustal heating. During an accretion outburst, deep crustal heating brings the entire crust out of thermal equilibrium with the core. When accretion ends and the neutron star enters quiescence, crust cooling powers an observable X-ray light curve [6–8]. Thermal evolution models of accreting neutron stars that include deep crustal heating successfully reproduce most observed quiescent X-ray light curves [9]. The cooling light curves of several sources, however, require an additional heat deposition in the outer crust during outburst to reach observed quiescent temperatures [10, 11]. The source of extra heating remains unknown, but must be comparable in strength to the heat release from non-equilibrium nuclear reactions.

Here we discuss a new source of heating in neutron star crusts from the decay of charged pions on the neutron star surface. The neutron star’s strong gravity accelerates incoming particles to kinetic energies of several hundred MeV per nucleon before they reach the neutron star surface. The accreted matter, usually consisting of hydrogen or helium, undergoes nuclear collisions with the nuclei on the neutron star surface. Nuclear collisions produce pions, in particular π^+ , that upon decay emit a flux of neutrinos. Approximately half of these neutrinos carry their energy into the crust, where they experience multiple scatterings and are eventually absorbed in the inner crust. This neutrino heating provides an additional source for deep crustal heating. In this work we present the first calculations of deep crustal heating by neutrinos from the decay of stopped pions on the surface of neutron stars.

The paper is organized as follows. In Section II we develop the formalism required to discuss the energy deposition by neutrinos from the stopped pion decays. We will first briefly review the main mechanism of deep crustal heating by neutrinos in II A. Following this discussion, in II B, we review the main steps involved in calculating the energy deposited from pion production on the surface of neutron stars. We close this Section by discussing in II C the approximate location of the inner crust where neutrinos will deposit their energies. We then proceed to Section III to display the results of our calculations using various equations of state (EOS) as well as pion production from three possible nuclear reactions. This section ends with a discussion of the observational implications of deep crustal heating in understanding cooling light curves of neutron stars in X-ray transients. Finally,

* fattoye@indiana.edu

† ebrown@pa.msu.edu

‡ andrew.cumming@mcgill.ca

§ adeibel@indiana.edu

¶ horowitz@indiana.edu

** bao-an.li@tamuc.edu

†† zidulin@imail.iu.edu

we offer our conclusions in Section IV.

II. FORMALISM

A. The Main Mechanism

Neutron stars in low-mass X-ray binaries typically accumulate hydrogen-rich or helium-rich matter from the surface of their companions in an accretion disk, a rotating disk of matter formed by accretion around the neutron star. The accumulated matter is later accreted onto the neutron star surface during an accretion outburst stage which makes neutron stars as bright X-ray sources. If the innermost stable orbit lies outside the neutron star, or if the accretion disk is truncated by the magnetic field of the star, the final trajectory of the accreted material can be close to radial, and the matter arrives at the neutron star surface with close to the free-fall velocity. For such quasi-spherical flows most of the gravitational potential energy is retained in the incoming particles in the form of the kinetic energy that particles carry into the neutron star. During outburst, these incoming particles collide with the nuclei on the neutron star surface [12] and can produce pions if the particle's kinetic energy is above the pion production threshold of ≈ 290 MeV. Neutral pions decay almost instantaneously via $\pi^0 \rightarrow 2\gamma$ releasing their energy at the surface. Neutrinos from the decay of negative pions may be strongly suppressed because π^- are often absorbed, via strong interactions, before they can undergo a weak decay. Positively charged pions slow down and stop near the neutron star surface and decay into muons and muon neutrinos through $\pi^+ \rightarrow \mu^+ \nu_\mu$. This produces monoenergetic muon neutrinos, ν_μ , of energy $E_{\nu_\mu} = 29.8$ MeV. The anti-muon subsequently decays through $\mu^+ \rightarrow e^+ \nu_e \bar{\nu}_\mu$ on a muon-decay time scale of $\tau = 2.2 \mu\text{s}$, with a well-determined neutrino energy spectrum [13]. Approximately half of the neutrinos produced escape the neutron star and the other half move into the crust carrying a total energy of

$$Q_\nu \approx 0.5 (E_{\nu_\mu} + E_{\nu_e} + E_{\bar{\nu}_\mu}) N_{\pi^+} = (50.4 \text{ MeV}) N_{\pi^+} \quad (1)$$

per accreted nucleon, where N_{π^+} is the total number of π^+ 's produced per accreted nucleon. In addition to gravitational acceleration, accreting particles may undergo electromagnetic acceleration in the strong electric and magnetic fields that are likely present. This could significantly increase pion and neutrino production, but we will explore this in later work.

B. Pion Production per Accreted Nucleon

We now calculate the number of charged pions produced from infalling matter. Assuming that the infalling matter has zero velocity at infinity (free-falling), we estimate the kinetic energy T of the accreted matter at the

surface of the neutron star [12] using

$$T = m_0 c^2 \left(\frac{1}{\sqrt{1 - R_S/R}} - 1 \right), \quad (2)$$

where $R_S \equiv 2GM/c^2$ is the Schwarzschild radius, m_0 is the mass of the infalling particle, and M and R are the neutron star mass and radius, respectively. If the kinetic energy of the incoming particles is sufficiently large, they will collide with the nuclei on the surface of the neutron star and can produce pions. The multiplicity of pion production, defined as the number of pions produced per collision event, strongly depends on the initial kinetic energy of the incoming particle as well as on the type of the target nuclei. Here the target nuclei on the surface of neutron stars could be composed of any mixtures of light-to-medium nuclei. Since both incoming protons and α -particles are charged particles, before they undergo a hard nuclear collision, they partially lose energy due to interaction with atmospheric electrons. The energy loss of charged particles can be calculated using the Bethe-Bloch equation

$$-\frac{dE}{dx} = K \frac{Z_p^2 Z_t}{\beta^2 A_t} \left(\frac{1}{2} \ln \frac{2m_e c^2 \beta^2 \gamma^2 T_{\text{max}}}{I^2} - \beta^2 - \frac{\delta}{2} \right), \quad (3)$$

where $K \approx 0.307075 \text{ MeV mol}^{-1} \text{ cm}^2$, Z_p is the charge number of the incident particle (projectile), Z_t is the atomic number of the target, A_t is the atomic mass of the target in g mol^{-1} , $\beta = v/c$, $\gamma = 1/\sqrt{1 - \beta^2}$ is the relativistic Lorentz factor, I is the mean excitation energy, and δ is the density effect correction to ionization energy loss which is negligible for energies under consideration. Here

$$T_{\text{max}} = \frac{2m_e c^2 \beta^2 \gamma^2}{1 + 2\gamma m_e/m_0 + (m_e/m_0)^2}, \quad (4)$$

is the maximum kinetic energy which can be imparted to a free electron in a single collision. A complete description of the electronic energy loss by heavy particles can be found in Chapter 32 of Ref. [14]. A similar study of the incident-beam particles deceleration through repeated Coulomb scatters from atmospheric electrons was also carried out in Ref. [12]. The energy of the particle that undergoes a hard nuclear collision is therefore

$$E_f(x) \approx E_i(x) + \lambda \frac{dE}{dx}, \quad (5)$$

where $\lambda = 1/n\sigma$ is the strong interaction mean free path, n is the number density of scattering centers, and σ is the strong collision cross section. Note that the energy loss $\frac{dE}{dx}$ depends on the initial beam energy $E_i(x)$ through Lorentz parameters. Therefore, Eqn. (5) takes an exact form if one replaces λ with $\Delta x = \lambda/N$, where $N \gg 1$, and solves the recurrent relation

$$E(x + \Delta x) = E(x) + \Delta x \frac{dE}{dx}, \quad (6)$$

for all x -values. The probability density function for the interaction of a particle after traveling a distance x in the medium is given by [15]

$$w(x) = \frac{1}{\lambda} e^{-x/\lambda} . \quad (7)$$

If the incident beam energy per nucleon during hard collision $E(x)$ is above the threshold energy of ≈ 290 MeV pions are produced. The pion production multiplicity, $\mu(E) = \sigma_\pi/\sigma_{\text{tot}}$, depends greatly on the kinetic energy of the incident particles as given by Eqn. (6). Here σ_π is the pion production cross section, whereas σ_{tot} is total reaction cross section. We discuss $\mu(E)$ in Sec. III. Then the total number of pions produced per infalling particle can be calculated as

$$N_{\pi^+} = \int_0^{x_{\text{max}}} \mu_{\pi^+}(E) w(x) dx , \quad (8)$$

where x_{max} is the range, or the maximum possible distance the incoming charged particle can penetrate the matter before losing all of its kinetic energy through electromagnetic energy loss.

C. Transport Optical Depth and Deep Crustal Heating

We want now to demonstrate a first-order rough estimation of the location in the crust where neutrinos deposit their energies. The neutrinos moving into the neutron star crust “forget” their original direction of motion after a succession of collisions and having been carried a distance corresponding to their transport mean free path which can be determined by the neutrino transport optical depth

$$\tau^{\text{tr}} = \int_0^l (\sigma_{\nu i}^{\text{tr}} \rho_i + \sigma_{\nu n}^{\text{tr}} \rho_n) dl' , \quad (9)$$

where $\sigma_{\nu i}^{\text{tr}}$ ($\sigma_{\nu n}^{\text{tr}}$) is the neutrino-ion (neutrino-free neutron) transport cross section, $n_{\text{ion}} = n/A$ is the ion number density in the crust, A is the number of nucleons in the unit cell, $n_n = N_f n_{\text{ion}}$ is the number density of free neutrons, and N_f is the number of free neutrons in a unit cell. The transport cross section is defined as

$$\sigma^{\text{tr}} = \int d\Omega \frac{d\sigma}{d\Omega} (1 - \cos \theta) , \quad (10)$$

with the free-space differential cross section for neutrino-nucleon elastic scattering given by [16]

$$\frac{d\sigma_{\nu n}}{d\Omega} = \frac{G_F^2 E_\nu^2}{4\pi^2} (C_v^2 (1 + \cos \theta) + C_a^2 (3 - \cos \theta)) , \quad (11)$$

where θ is the scattering angle, E_ν is the incoming neutrino energy, C_v is the vector coupling constant, and C_a

is the axial vector coupling constant. The neutrino-ion elastic scattering differential cross section is

$$\frac{d\sigma_{\nu i}}{d\Omega} = \frac{G_F^2 E_\nu^2}{4\pi^2} (1 + \cos \theta) \frac{Q_w^2}{4} F(Q^2)^2 , \quad (12)$$

where $Q_w = NQ_w^n + ZQ_w^p$ is the total weak charge of the ion with $Q_w^n = -0.9878$ and $Q_w^p = 0.0721$, $F(Q^2)$ is the ground state elastic form factor of the ions [17]

$$F(Q^2) = \frac{1}{Q_w} \int d^3r \frac{\sin(Qr)}{Qr} [\rho_n(r) - (1 - 4 \sin^2 \theta_W) \rho_p(r)] , \quad (13)$$

with $Q^2 = 2E_\nu^2(1 - \cos \theta)$ being the four momentum transfer squared and θ_W is the Weinberg angle.

Notice that both $\sigma_{\nu i}^{\text{tr}}$ and $\sigma_{\nu n}^{\text{tr}}$ are functions of the neutrino energy. The neutrino energy spectrum from stopped pions is well known [13]. To determine the neutrino-ion and neutrino-free neutron elastic scattering cross sections we use the root-mean-square neutrino energies calculated as

$$E_\nu^{\text{rms}} = \left(\frac{\int E^2 \Phi(E) dE}{\int \Phi(E) dE} \right)^{1/2} , \quad (14)$$

where $\Phi(E)$ is the neutrino flux with energy E [13]. In particular, we use the root-mean-squared values of $E_{\nu_e}^{\text{rms}} = 33.3$ MeV and $E_{\nu_\mu}^{\text{rms}} = 37.7$ MeV for electron and muon neutrinos, respectively (see Eqn. (1)) and $E_{\nu_\mu} = 29.8$ MeV.

By definition, τ^{tr} which is given by Eqn. (9) represents the number of transport mean free paths for the neutrino traveling from the surface of the star at $l = 0$ to some inner depth l . Neutrinos are assumed to “forget” their original direction of motion at a depth of $l = \Delta R$ corresponding to $\tau^{\text{tr}} \approx 1$. As a first-order rough estimate, one can assume neutrinos eventually deposit their energies around this optical depth.

Electron neutrinos are most likely absorbed in the crust via inelastic neutrino charged current interactions (*e.g.* $\nu_e + n \rightarrow p + e^-$, or $\nu_e + X_Z^A \rightarrow X_{Z+1}^A + e^-$). Whereas muon (anti)neutrinos deliver most of their energies through muon (anti)neutrino-electron scatterings, *i.e.*

$$\begin{aligned} \nu_\mu + e^- &\rightarrow \nu'_\mu + e^{-'} , \\ \bar{\nu}_\mu + e^- &\rightarrow \bar{\nu}'_\mu + e^{-'} . \end{aligned}$$

One can estimate the average fractional energy loss for muon neutrinos interacting with electrons at rest as well as for the degenerate gas of electrons [18]. These estimations show that in about tens of electron scatterings, the muon (anti)neutrinos will lose most of their energies, and will eventually leave the star as their energy becomes low enough corresponding to a very small cross-section, hence a very large neutrino mean free path.

Another possible channel for neutrinos to deposit their energies could be through a charged-current reaction $\nu_\mu + e^- \rightarrow \mu^- + \bar{\nu}_e$. This is because the transport optical depth corresponds to the density regions in the crust

where muon threshold can be reached. Notice that for non-energetic neutrinos the muon threshold is usually at a much higher densities. Other possible channels such as the neutrino-neutron scattering might not be as important as neutrino-electron scatterings. That is because although the cross-section for neutrino-neutron scattering is much bigger than the neutrino-electron scattering, the amount of energy deposited by a single neutrino-neutron scattering is much smaller than the one by a single neutrino-electron scattering. Finally, one can think of inelastic neutral current neutrino-nucleus scattering as a potentially interesting channel for neutrino energy deposition. This has been discussed at supernovae neutrino energies and is believed to be important for supernovae simulations [19]. However, more works are needed to be done to determine whether this is a robust channel for neutrino energy deposition in the neutron star crust. Thus, it is safe to conclude that as a first-order rough estimate most of the energy of Q_ν given by the Eqn. (1) is delivered to the inner crust of depths of about $\sim \Delta R$.

III. RESULTS

A. Equations of State of Neutron-Star Matter

As noted earlier, the multiplicity of pion productions strongly depends on the kinetic energy of the incoming particles, which in turn depends on the compactness parameter, R_S/R . Since the stellar compactness is strongly sensitive to neutron-star equation of state, for realistic considerations we will consider a set of the equations of state that are consistent with current nuclear experimental and observational constraints. Moreover, a detailed knowledge of the equation of state of the crust is important in calculations of the transport optical depth.

The equation of state adopted in this work is composed of several parts. Matter in the outer crust of the neutron star is organized into a Coulomb lattice of neutron-rich nuclei embedded in a degenerate electron gas. The composition in this region is solely determined by the masses of neutron-rich nuclei in the region of $26 \leq Z \lesssim 40$ and the pressure support is provided primarily by the degenerate electrons. For this region we adopt the equation of state by Haensel, Zdunik and Dobaczewski (HZD) [20]. The inner crust begins at the neutron-drip density of $\rho_{\text{drip}} \approx 4 \times 10^{11} \text{ g cm}^{-3}$. The EOS for the inner crust at mass densities $\rho > \rho_{\text{drip}}$ is, however, highly uncertain and must be inferred from theoretical calculations. In addition to a Coulomb lattice and an electron gas, the inner crust now includes a dilute vapor of quasi-free neutrons. Moreover, at the bottom layers of the inner crust, complex and exotic structures with almost equal energies referred to as “nuclear pasta” have been predicted to emerge [21–23]. For this region we use the EOS by Negele and Vautherin [24]. The inner crust ends at a mass density near $\rho_t \approx 1.3 \times 10^{14} \text{ g cm}^{-3}$, beyond which the neutron star matter becomes uniform. For this uni-

form liquid core region we assume two equations of state that cover a wide range of uncertainties that currently exist in the determination of the equation of state of nuclear matter at normal and supra nuclear densities:

- The relativistic mean-field model by Chen and Piekarewicz [25] (*FSU2*), whose parameters were calibrated to reproduce the ground-state properties of finite nuclei and their monopole response, as well as to account for the maximum neutron star mass observed to date [26–28]. Due to the lack of stringent isovector constraints, the original *FSU2* predicts a relatively stiff symmetry energy of $J = 37.6 \pm 1.1 \text{ MeV}$ with density slope of $L = 112.8 \pm 16.1 \text{ MeV}$. It is known that by tuning two purely isovector parameters of the RMF model one can generate a family of model interactions that have varying degrees of softness in the nuclear symmetry energy without compromising the success of the model in reproducing ground-state properties [29, 30]. Following this scheme we tuned the purely isovector parameters of the *FSU2* model to get $J = 31.1 \text{ MeV}$ and $L = 50.0 \text{ MeV}$ and refer to this model as the *FSU2* (soft). The maximum neutron-star masses predicted by these models are $2.07M_\odot$ and $2.03M_\odot$, respectively.
- The soft and stiff equations of state that agree with the lower and upper limits of the EOS band derived from microscopic calculations of neutron matter are based on nuclear interactions from chiral effective field theory by Hebeler *et al.* [31] (*HLPS*). Notice that the symmetry energy parameters in this model are $29.7 < J < 33.5 \text{ MeV}$ and $32.4 < L < 57.0 \text{ MeV}$. Similarly, the maximum stellar masses predicted by these models are $2.04M_\odot$ and $2.98M_\odot$, respectively.

Model	R_{14} (km)	T_{14} (MeV)	R_{20} (km)	T_{20} (MeV)
<i>FSU2</i> (soft)	12.89	200.5	12.03	377.2
<i>FSU2</i> (stiff)	14.10	178.0	12.95	334.2
<i>HLPS</i> (soft)	9.95	289.5	9.68	565.2
<i>HLPS</i> (stiff)	13.59	186.8	14.14	291.6

TABLE I. The radii R of a 1.4– and 2.0 M_\odot neutron stars as well as the incoming kinetic energies of a nucleon (with mass of $m_N = 939 \text{ MeV}$) at the surface of neutron stars T predicted by the four equations of state discussed in the text.

A recent survey on the mass spectrum of compact objects in X-ray binaries from 19 sources shows that their masses can be anywhere in the range of $M = (0.9 - 2.7) M_\odot$ [32]. Note that stars made with stiff equations of state can accelerate particles to near the pion-production threshold only for more massive stars, whereas those with soft equations of state allow particles to gain kinetic energies significantly larger than the pion-production threshold even for low-mass neutron stars (see Table I).

B. Production of π^+ in p - p , p - Fe and α - Fe Collisions

In this subsection we will discuss the sensitivity of the pion production to the incoming energy of the particle and to the target nuclei. We assume that the accreted matter (incoming particles) is composed of either protons or helium. The surface composition of neutron stars (target nuclei) however remains an outstanding problem [33]. For accreting neutron stars, the upper layer is likely composed of lighter elements such as hydrogen or helium, depending on the composition of accreted material from the companion star. Ultra-compact low mass X-ray binaries with orbital periods of tens of minutes accrete from a hydrogen-deficient companion that can be a He, C-O, or O-Ne-Mg white dwarf, so that the neutron star surface composition would consist of heavier elements than H or He, *e.g.* see Ref. [34]. For the sake of simplicity, instead of a range of target nuclei, we assume only two types of the target nuclei, protons and Fe , and only a select nuclear collisions: p - Fe , p - p , and α - Fe .

Charged pion production from the interaction of proton beams with some selected nuclei have been measured at incident energies of 585 MeV [35], 730 MeV [36], as well as at 800 and 1600 MeV [37, 38]. Inclusive pion production at lower incident energies of 330, 400, and 500 MeV from proton-nucleus collisions (^{12}C and ^{138}U) nuclei have also been measured. However, measurements of pion production cross sections at medium beam energies for proton-nucleus collisions are still incomplete.

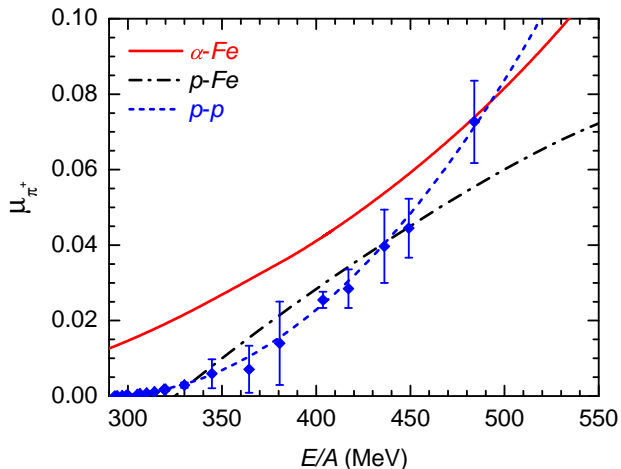


FIG. 1. (Color online) The multiplicity of pion production as a function of beam energy for p - Fe collisions (dash-dotted black line) estimated using the Monte-Carlo results of Ref. [39] and for p - p collisions (dashed blue line) which is a polynomial fit to the experimental data from [40–43] (blue diamond symbols). Also shown is π^+ multiplicities from the isospin-dependent Boltzmann-Uehling-Uhlenbeck (IBUU) transport simulations in the α - Fe collision (solid red line).

Based on the available experimental data Ref. [39] performed a Monte-Carlo simulation to evaluate the total

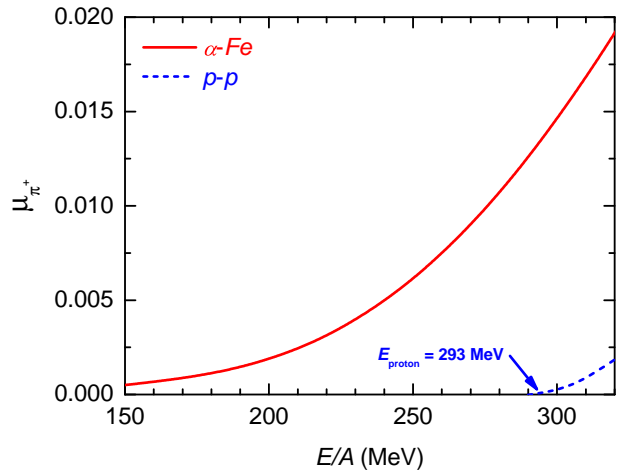


FIG. 2. (Color online) Same as Fig. 1 but now for ‘subthreshold’ energies.

pion production cross sections at various proton beam energies on selected nuclei. Using these Monte-Carlo data and the p - Fe reaction cross sections we estimated pion multiplicities for p - Fe collision at incident beam energies above 325 MeV, see Fig. 1. Note that the pion production cross section in Monte-Carlo simulations is assumed to go to zero at energies below 325 MeV [39]. It is important to mention, however that pions can be produced at subthreshold energies via the excitation and decay of Δ -resonances (See Ref. [44] and references therein). The Fermi motion of nucleons in nuclei can also greatly enhance the pion production cross sections in the vicinity of the threshold energy [45, 46]. Despite efforts to measure subthreshold pion production in the past (See, Ref. [47] and references therein), regrettably, experimental data on this front still remains incomplete.

For stars that accrete hydrogen from the companion, the p - p collision becomes an interesting case [12, 48] to study the pion production. Fortunately, there are sufficient experimental data available on the pion production in p - p collisions. Using the experimental data from [40–43] we plot the multiplicity of pion production as a function of the proton beam energy from the p - p collisions (see Fig. 1). The current experimental error-bars are in the order of 25% for most of these measurements, except for few cases when beam energies are in the range of $344.6 < E < 380.6$ MeV, the relative error-bars are as large as $\simeq 80\%$.

On the other hand, experimental measurements of pion production in α - Fe collisions are still missing. For this we use the IBUU transport model to calculate π^+ multiplicities at various incident beam energies per nucleon and impact parameters. For a detailed description of this transport model we refer the reader to Ref. [49, 50]. The results are presented in Fig. 1 alongside p - Fe and p - p collisions. In Fig. 2 we display predicted π^+ multiplicities as a function of the incident beam energies per nucleon for

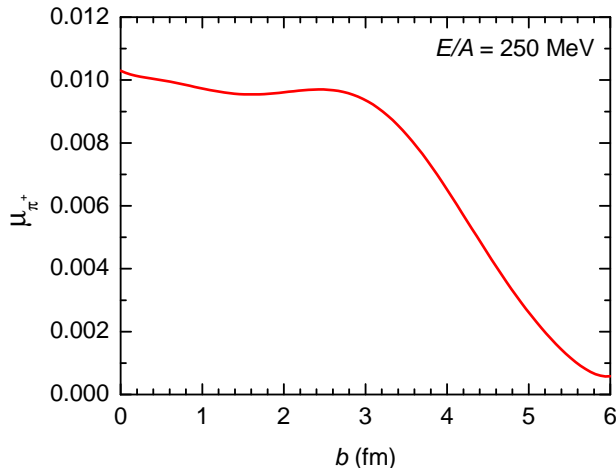


FIG. 3. (Color online) The π^+ multiplicity in α -Fe collisions versus impact parameter b for incident α energies per nucleon of $E/A = 250$ MeV calculated using IBUU transport simulations.

subthreshold energies. For comparison, we also show the results from p - p collisions in the lower right corner. In this model all subthreshold pions are produced from decays of low-mass $\Delta(1232)$ resonances formed in nucleus-nucleus inelastic collisions. While the pion production cross sections drop sharply when the energy per nucleon is below threshold, there is an appreciable pion production cross section at incident beam energies as low as 150 MeV per nucleon mostly due to Fermi motion of nucleons in Fe . Note that pion production in heavy-ion collisions depends on the EOS and the ratio of charged pions on the nuclear symmetry energy used. In this exploration study, we use a momentum-independent potential corresponding to a stiff EOS with $K_0 = 380$ MeV and a symmetry energy that is linear in density. In our calculation for α - Fe collisions, we used μ_{π^+} multiplicities averaged over the impact parameter b :

$$\mu_{\pi^+, \text{ave}} = \frac{\int_0^{b_{\text{max}}} \mu_{\pi^+}(b) b db}{\int_0^{b_{\text{max}}} b db}, \quad (15)$$

whose dependence is plotted in Fig. 3. For head-on collisions with $b = 0$ fm the pion-production cross section is obviously much larger. In generating these data we run 100,000 events for most cases, except for low incident energies, where we used up to 300,000 events to have a better statistics. The statistical error-bars for these simulations are of the order of $\approx 30\%$. It is worth noting that uncertainties coming from different EOS models and the density dependence of the symmetry energy are of the same order as the statistical errors quoted above. The detailed model dependencies near the pion production threshold are addressed in Ref. [51].

C. Neutrino Energy Deposition in the Inner Crust

Model	Q_{ν}^{pp} (MeV)	Q_{ν}^{pFe} (MeV)	$Q_{\nu}^{\alpha Fe}$ (MeV)
<i>FSU2</i> (stiff)	0.009 [0.000]	0.005 [0.000]	0.258 [0.004]
<i>FSU2</i> (soft)	0.069 [0.000]	0.131 [0.000]	0.493 [0.009]
<i>HLPS</i> (stiff)	0.000 [0.000]	0.000 [0.000]	0.114 [0.006]
<i>HLPS</i> (soft)	2.114 [0.000]	1.963 [0.000]	2.822 [0.109]

TABLE II. The total energy per accreted nucleon deposited by neutrinos in the inner crust for a 2.0 [1.4] M_{\odot} neutron star using the four equations of state discussed in the text and for three possible reactions: pp , p - Fe , and α - Fe .

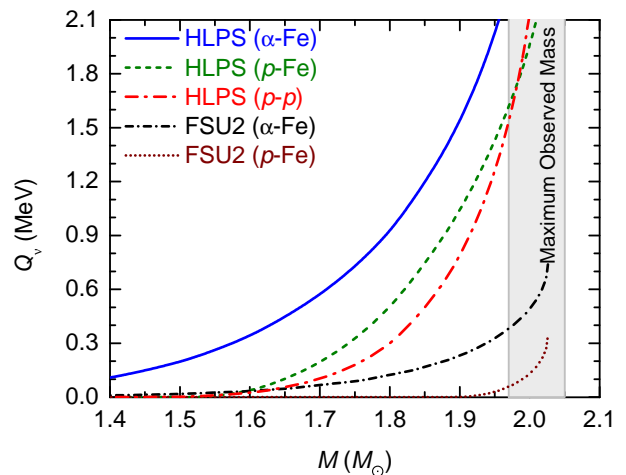


FIG. 4. (Color online) The total energy deposited by neutrinos into the inner crust as a function of neutron star mass for the soft EOSs discussed in the text: *HLPS* (soft) and *FSU2* (soft).

We now calculate the total energy carried by neutrinos into the inner crust. In Table II we present results for a $2M_{\odot}$ and for a $1.4M_{\odot}$ (in square brackets) neutron star and the four equations of state discussed in the text. In Fig. 4 we display the full results as a function of the neutron star mass for soft equations of state only. As is also evident from Table I, low-mass neutron stars can accelerate the infalling matter to energies of about the pion-production threshold only. Therefore the result is highly sensitive to the pion production cross section around threshold energies. This result calls for improved experimental measurements of pion production in proton-proton collisions, as well as for pion production in p - Fe and α - Fe collisions for beam energies per nucleon in the range of 150 to 600 MeV.

Moreover, there is a strong sensitivity of the pion production to the equation of state employed in determination of stellar structure. In particular, if the equation of state is very stiff—such as the *HLPS* (stiff)—then even for a $2M_{\odot}$ neutron star the incoming particles are not accelerated enough to produce pions (See Tables I and

Model	M (M_\odot)	$\rho_{\bar{\mu}}$ (10^{12} g cm $^{-3}$)	$y_{\bar{\mu}}$ (10^{16} g cm $^{-2}$)	$\Delta R_{\bar{\mu}}$ (km)	ρ_e (10^{12} g cm $^{-3}$)	y_e (10^{16} g cm $^{-2}$)	ΔR_e (km)	ρ_μ (10^{12} g cm $^{-3}$)	y_μ (10^{16} g cm $^{-2}$)	ΔR_μ (km)
<i>FSU2</i> (soft)	1.4	5.0	3.2	0.60	6.1	3.9	0.62	7.1	4.7	0.63
	2.0	9.7	4.0	0.31	11.3	5.0	0.31	12.9	6.1	0.32
<i>HLPS</i> (soft)	1.4	7.4	4.0	0.34	8.5	4.6	0.35	10.4	5.6	0.35
	2.0	16.5	5.0	0.17	18.7	6.1	0.17	20.7	7.4	0.18

TABLE III. The location in the neutron star inner crust, where neutrino transport optical depth equals $\tau^{\text{tr}} = 1$. Here $\rho_{\bar{\mu}}$, ρ_e , and ρ_μ are the mass density of the neutron-star matter in the crust where neutrinos with different flavors are first scattered (or absorbed), $y = P/g$ and ΔR are the corresponding column depth [9] and radial depth, where P is the local pressure and g is the local gravitational acceleration [52] at $r = R - \Delta R$.

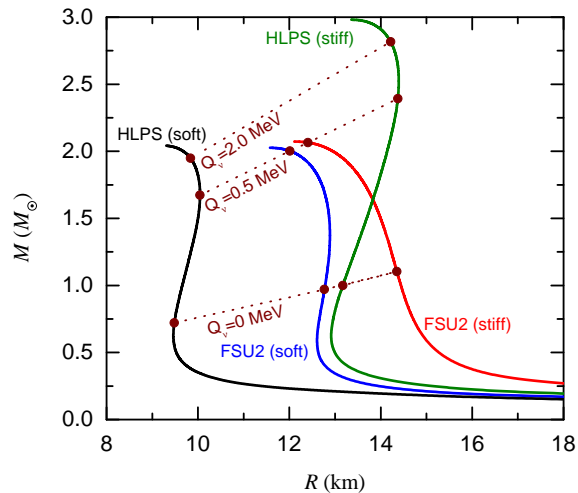


FIG. 5. (Color online). Mass-vs-Radius relation predicted by the four EOS models discussed in the text. The contours of constant neutrino heat deposits are shown with dotted curves.

II). On the other hand, if the equation of state is soft, then for a $M = 2M_\odot$ neutron star the energy deposited by neutrinos can be as large as $Q_\nu \simeq 2.8$ MeV per accreted nucleon. The result is more pronounced if helium is being accreted onto the surface of neutron star, mainly because the IBUU simulations suggest that a substantial amount of pions can be produced at subthreshold beam energies. In Fig. 5 we plot the Mass-vs-Radius relation predicted by the four equations of state, where the contours of $Q_\nu = 0, 0.05,$ and 2.0 MeV's coming from α -Fe collisions are plotted. As evident from the figure, the heating gets more pronounced for massive and/or compact stars only.

Finally, let us investigate the impact of the neutron star's compactness parameter on the amount of heat deposition. While stars built with the *HLPS* (stiff) equation of state may not accelerate the infalling matter to high kinetic energies for low-mass stars, it can certainly do so for very massive neutron stars. In particular, for a $M = 2.8M_\odot$, the total energy deposit is $Q_\nu = 1.89$ (1.33) MeV, when α -Fe (p -Fe) collisions take place at the surface (Also see Fig. 5). To cover all possible equations of state in Fig. 6 we plot the results as a function of the compactness parameter.

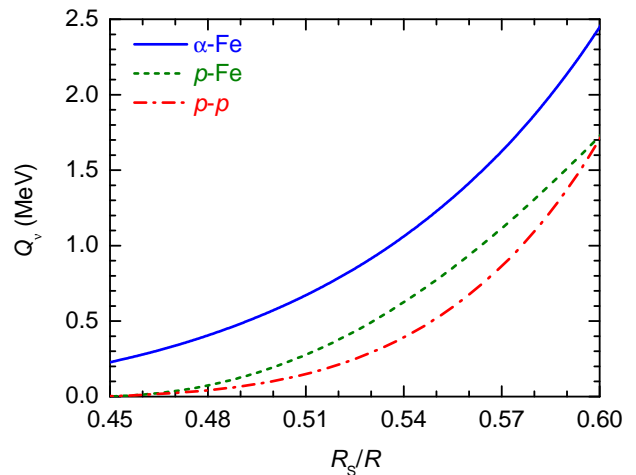


FIG. 6. (Color online) The total energy deposited by neutrinos into the inner crust as a function of neutron star compactness, R_s/R .

We find that the heat deposition from neutrinos is comparable with other previously known sources of deep crustal heating such as from pycnonuclear fusion reactions. In Table III we present our results for the approximate location in the neutron star inner crust, where neutrino transport optical depth equals to 1. The results are presented for the more interesting cases of soft equations of state only, where Q_ν is significant even for moderate-mass neutron stars. Depending on the mass of the star and the EOS model used, the energy of Q_ν is delivered to the regions of the inner crust where mass densities are of the order 10^{12} to 10^{13} g cm $^{-3}$. For example, for a $2M_\odot$ neutron star this would correspond to mass densities of $9.69 < \rho_{12} < 20.74$ in units of 10^{12} g cm $^{-3}$, or equivalently to baryon densities of $0.036 < \rho/\rho_0 < 0.078$, where $\rho_0 \approx 2.66 \cdot 10^{14}$ g cm $^{-3}$ is the nuclear saturation density.

Obviously, $\tau^{\text{tr}} = 1$ is only a rough estimate for the location of the neutrino heat deposition. Moreover, Table III assumes that half of the neutrinos produced from the decay of stopped pions travel radially inward. In reality, the decay is isotropic and therefore it is worth to analyze the approximate location of heat delivery as an angle of incidence of neutrinos. The fraction of the number of neutrinos within a cone with apex angle 2θ to the total

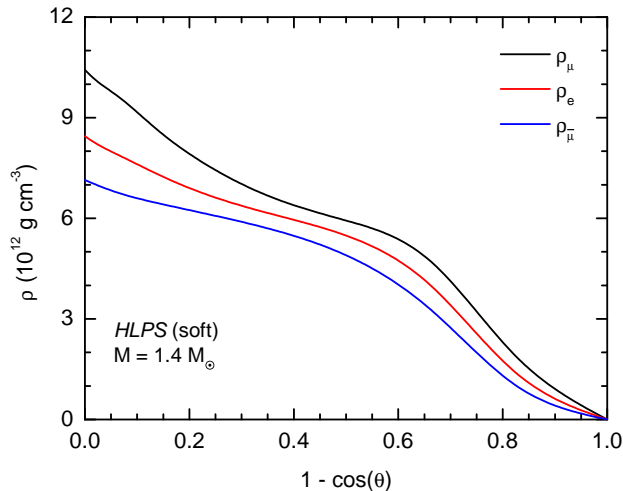


FIG. 7. (Color online) The location in the neutron star inner crust, where neutrino transport optical depth equals $\tau^{\text{tr}} = 1$ for different angles of incidence θ .

number of neutrinos is equal to $x = \frac{1}{2}(1 - \cos\theta)$. Here $\theta = 0$ corresponds to the angle of incidence in the radial direction, whereas $\theta = \frac{\pi}{2}$ corresponds to the direction horizontal to the surface. In Fig. 7 we display the location of heat deposition as a function of $1 - \cos\theta$ for a $1.4M_{\odot}$ neutron star using *HLPS* (soft) EOS. The result shows that most of neutrinos are delivered to the deep region of the crust, and only a small fraction of them scatter at shallower regions.

Note that in our calculations above we did not take into account additional redshift effects as neutrinos go deeper into the crust. The effective neutrino energy should slightly increase due to the gravitational redshift by a factor of $e^{-\phi(r)/c^2} \sqrt{1 - R_S/R}$, where $\phi(r)$ is the local gravitational potential [52]. However our calculations show this effect is $\lesssim 2\%$ because the crust is thin.

D. Observational Implications

In this section, we will discuss observational implications of the extra heating from neutrinos in the presence of other sources of deep crustal heating. We will first discuss general implications for neutron stars cooling observation and then apply our result to a particular neutron star MXB 1659-29.

1. Cooling neutron stars

Non-equilibrium nuclear reactions during active accretion heat the neutron star crust out of thermal equilibrium with the core. When accretion stops, the crust cools toward thermal equilibrium with the core [6, 7, 53, 54]. Crust cooling is observed as a quiescent X-ray light curve, with one of the most well studied examples being the

cooling transient MXB 1659-29 [6, 9, 53, 54]. Cooling observations at successively later times into quiescence probes successively deeper layers in the crust with increasingly longer thermal times [9]. In particular, it was shown that about a year into quiescence the shape of the cooling light curve is sensitive to the physics at mass densities greater than neutron drip $\rho > \rho_{\text{drip}}$ corresponding to the inner crust [55]. This suggests that cooling light curves of neutron stars in low-mass X-ray binaries one-to-three years after accretion outbursts should be sensitive to the additional deep crustal heating by neutrinos [9].

Comparing our results with the heat released from pycnonuclear fusion reactions [5] we notice that not only are they of the same order, but also the heat is deposited in the same density regions (crust layer). Subsequently we calculated the column depths where neutrinos are first scattered, $y = \int_r^{\infty} \rho dr \approx P/g$ [9]. Here P is the local pressure and the neutron star's surface gravity is $g = (GM/R^2)(1 - 2GM/Rc^2)^{-1/2}$. We find that the column depth values lie in the range of $4.0 \cdot 10^{16} < P/g < 7.4 \cdot 10^{16} \text{ g cm}^{-2}$ (See Table III). Since the amount of heat deposited for massive stars is comparable to the heat released from pycnonuclear reactions, the observation of cooling light curves, in particular, could be used to help distinguish massive stars from the low-mass stars.

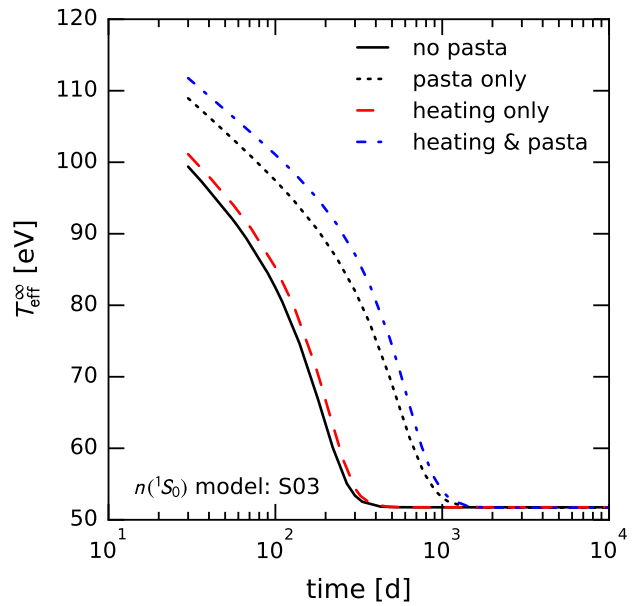


FIG. 8. (Color online) The redshifted surface temperature in units of eV as a function of time into quiescence. For the details of each curve please refer to the text.

To analyze the sensitivity of crustal heating by neutrinos on the cooling curves, we simulate the thermal evolution of a $2M_{\odot}$ neutron star crust using the thermal evolution code *dStar* [56], which solves the fully general

relativistic heat diffusion equations

$$\frac{\partial}{\partial t} \left(T e^{\phi/c^2} \right) = e^{2\phi/c^2} \frac{\epsilon_{\text{in}} - \epsilon_{\text{out}}}{C} - \frac{\frac{\partial}{\partial r} \left(L e^{2\phi/c^2} \right)}{4\pi r^2 \rho C (1+z)} \quad (16)$$

$$L e^{2\phi/c^2} = - \frac{4\pi r^2 K e^{\phi/c^2}}{1+z} \frac{\partial}{\partial r} \left(T e^{\phi/c^2} \right), \quad (17)$$

where ϵ_{in} is the nuclear and/or neutrino heating emissivity and ϵ_{out} is the neutrino emissivity from the core, C is the specific heat, K is the thermal conductivity and $1+z = [1 - 2GM/(rc^2)]^{-1/2}$ is the gravitational redshift factor. The detailed microphysics of the crust is discussed in Ref. [9] and the parameters of the cooling model are described in Ref. [57]. In particular, the core neutrino emissivity ϵ_{out} includes the modified and direct Urca reactions that may impact quiescent crust cooling at late times depending on the core's heat capacity [58]. Though the core's heat capacity remains unknown, long term monitoring observations can be used to place a lower limit on its value [59]. This model also assumes an impurity parameter of $Q_{\text{imp}} = 1.0$ throughout the crust, which is defined as

$$Q_{\text{imp}} = \frac{1}{n_{\text{ion}}} \sum_i n_i (Z_i - \langle Z \rangle)^2, \quad (18)$$

where n_i is the number density of the nuclear species with Z_i number of protons, and $\langle Z \rangle$ is the average proton number of the crust composition.

In Fig. 8 we display the crust cooling curves for four possible cases. The solid black curve corresponds to the case without heat deposition from neutrinos in the inner crust with $Q_{\text{imp}} = 1.0$. The red dashed curve corresponds to the case when a 2.0 MeV per accreted nucleon heat source is deposited at density regions of $10^{12} < \rho < 10^{13} \text{ g cm}^{-3}$. The crust temperature is marginally increased by the neutrino heating because most of the additional heat is transported into the core.

We then examine two cases, with and without neutrino heating, but including a nuclear pasta layer in the inner crust. It is expected that nuclear pasta forms at densities above $\rho > 8.0 \cdot 10^{13} \text{ g cm}^{-3}$ corresponding to the bottom layers of the inner crust. The thermal conductivity of nuclear pasta could be small, corresponding to a large impurity parameter [60]. The black short-dashed curve shows the case of no neutrino heating, but $Q_{\text{imp}} = 20$ at densities of $\rho > 8.0 \cdot 10^{13} \text{ g cm}^{-3}$ corresponding to nuclear pasta. Finally, in blue dash-dotted line we display a cooling curve that includes both nuclear pasta and the heat deposition from neutrinos. The crust temperature is higher in these two cases, because the low thermal conductivity of the nuclear pasta layer prevents a large portion of heat from diffusing into the core.

As evident from Fig. 8, the additional heat source can make a noticeable change in the cooling light curves. The cooling rate depends on many other factors and in particular strongly depends on the crust thickness, which is usually small for massive stars. Moreover, as illustrated

in Fig. 8 the low thermal conductivity corresponding to the nuclear pasta can strongly affect thermal diffusion time maintaining a temperature gradient between the neutron star's inner crust and core for several hundred days into quiescence [57]. Note that all of the above models use the same pairing gap model of neutron superfluid in the 1S_0 singlet state with the critical temperature profile given by Schwenk *et al.* [61]. We have also tested other superfluid pairing gap models, such as the one by Gandolfi *et al.* [62], and the results are qualitatively similar to Fig. 8.

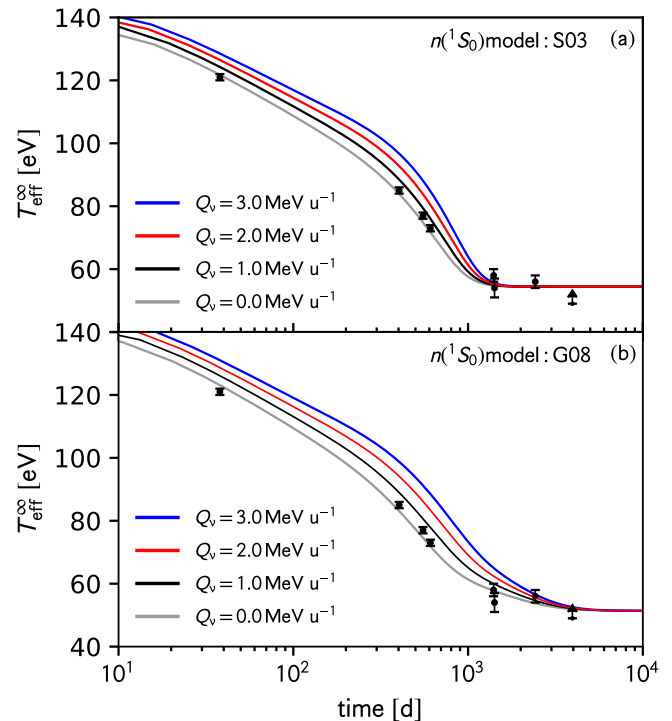


FIG. 9. (Color online) Observed cooling light curve of MXB 1659-29 (black data points) [63] and thermal evolution models for three cases of neutrino heating. (a) Crust cooling models with the S03 pairing gap and no nuclear pasta. The models use an impurity parameter of $Q_{\text{imp}} = 3$ for the entire crust and a core temperature of $T_{\text{core}} = 4.2 \times 10^7 \text{ K}$. (b) Crust cooling models with the G08 pairing gap and nuclear pasta. The models use an impurity parameter of $Q_{\text{imp}} = 1$ for the crust and a $Q_{\text{imp}} = 20$ layer representing nuclear pasta at mass densities $\rho \geq 8 \times 10^{13} \text{ g cm}^{-3}$. These models have a core temperature of $T_{\text{core}} = 3.75 \times 10^7 \text{ K}$.

2. Crust cooling in MXB 1659-29

As described above, neutrino deep crustal heating will noticeably increase the crust temperature and the shape of the cooling light curve. Here we investigate the impact of extra heating from neutrinos on the particular case of MXB 1659-29 that entered quiescence after an ≈ 2.5 year accretion outburst [63–65] and cooled for ≈ 4000 days

before entering outburst once more [66]. The late time cooling observations probe the thermal properties of the inner crust and make MXB 1659-29 an interesting test case for neutrino heating.

Our thermal evolution model of MXB 1659-29 uses a $M = 1.6 M_{\odot}$ and $R = 11.2 \text{ km}$ neutron star at the observed outburst accretion rate of $\dot{m} \approx 0.1 \dot{m}_{\text{Edd}}$. The model includes a $Q = 1 \text{ MeV}$ per accreted nucleon shallow heat source between $y = 2 \times 10^{13} \text{ g cm}^{-2}$ and $y = 2 \times 10^{14} \text{ g cm}^{-2}$, consistent with the findings from [9]. Using a model without nuclear pasta, the cooling light curve is fit with an impurity parameter for the entire crust of $Q_{\text{imp}} = 3$ and the S03 pairing gap [61]. We then test representative values of neutrino heating: 1, 2, and 3 MeV per accreted nucleon. As can be seen in Fig. 9, the model fit with $Q_{\text{imp}} = 3$ becomes inconsistent with the observational data once neutrino heating is added to the inner crust. In order to reestablish a fit, the crust impurity parameter must be lowered to $Q_{\text{imp}} < 3$ (corresponding to a higher crust thermal conductivity) as Q_{ν} increases.

Alternatively, the cooling of MXB 1659-29 may be fit with a nuclear pasta layer in the crust if the G08 pairing gap model is used [62], as we demonstrate in panel (b) of Fig. 9. In this case, the low thermal conductivity of the nuclear pasta maintains a higher crust temperature during quiescence and a layer of normal neutrons forms at the base of the crust [57]. Without neutrino heating, the cooling observations of MXB 1659-29 are fit with a crust impurity of $Q_{\text{imp}} = 1$ and a pasta impurity parameter of $Q_{\text{imp}} = 20$. We find that, similar to the model without nuclear pasta, as neutrino heating is increased in the inner crust, the pasta impurity parameter must decrease to reestablish a fit to the observations.

Note that the cooling of MXB 1659-29 may be fit with other neutron star masses and radii [9] and the results in Fig. 9 are for a fixed gravity in the neutron star crust (and crust thickness). Therefore our studies above are qualitative only as the amount of neutron heating for a $M = 1.6 M_{\odot}$ and $R = 11.2 \text{ km}$ neutron star from α - Fe collision in particular is just about 0.13 MeV and is bigger only for more massive and/or compact stars (See also Fig. 5). Cooling light curve shapes are degenerate in several parameters, for example: the neutron star gravity, the crust impurity parameter, and the mass accretion rate. Because the effect of neutrino heating is difficult to delineate from the effects of other model parameters we therefore can not determine if neutrino heating is present during outburst. It is worth noting, however, that if deep crustal heating from neutrinos is present then existing constraints derived from cooling light curves will need to be revisited, likely requiring a higher crust thermal conductivity or a different neutron star gravity.

IV. CONCLUSION AND OUTLOOK

We presented a new mechanism of deep crustal heating of neutron stars in mass-transferring binaries by neutrinos that are decay remnants of charged pions produced at the surface of neutron stars. Our calculations showed that massive and compact stars can accelerate infalling matter to energies substantially larger than the pion-production threshold resulting in ample generation of neutrinos. Approximately half of these neutrinos travel into the inner crust and deposit $\approx 1\text{--}2 \text{ MeV}$ per accreted nucleon for massive and compact stars.

The deep crustal heating from neutrinos is comparable in strength to pycnonuclear fusion reactions and other non-equilibrium nuclear reactions taking place during active accretion. Additional deep crustal heating will affect the cooling light curves of accreting neutron stars at late times $\gtrsim 300$ days into quiescence. The effect is most pronounced when the star is massive and might help distinguish high-mass stars from low-mass stars. In general, for a fixed gravity in the neutron star crust we find that additional deep crustal heating requires a higher thermal conductivity for the crust and the crust impurity parameter must be lowered. In the particular case of MXB 1659-29, for a model without nuclear pasta and the S03 pairing gap, $Q_{\text{imp}} \lesssim 3$ is required if any neutrino heating is added. For a model with nuclear pasta and the G08 pairing gap, $Q_{\text{imp}} \lesssim 20$ for nuclear pasta is needed if neutrino heating is present.

Our calculation of pion production assumes that the incoming protons are slowed by Coulomb collisions with atmospheric electrons [67]. Plasma instabilities or a collisionless shock may instead stop the proton beam (*e.g.* see Ref. [68]), reducing the rate of nuclear collisions. In addition, depending on the accretion geometry, the incoming particles may not have the full free-fall velocity, *e.g.* in disk accretion if the disk reaches all the way to the neutron star surface. Neutrino heating may operate only with a quasi-spherical accretion flow or if the neutron star lies within the last stable orbit (*e.g.* see discussion in Ref. [69]).

There is also a strong sensitivity of our results to the pion production cross sections at near threshold energies. Pion production may play a significant role in stellar environments and in particular, a better knowledge of pion production cross sections in p - p , p - Fe , α - α , and α - Fe reactions at beam energies 150-600 MeV/nucleon may help to better understand the structure and transport properties of neutron star crusts from cooling observations.

ACKNOWLEDGMENTS

We thank Professors Hans-Otto Meyer, Hendrik Schatz, and Rex Tayloe for many helpful discussions. F.J.F., C.J.H., and Z.L. are supported by the U.S. Department of Energy (DOE) grants DE-FG02-87ER40365 (Indiana University), de-sc0008808 (NUCLEI SciDAC Collaboration) and by the National Science Founda-

tion through XSEDE resources provided by the National Institute for Computational Sciences under grant TG-AST100014. E.F.B. is supported by the US National Science Foundation under grant AST-1516969. A.C. is supported by an NSERC Discovery Grant and is a mem-

ber of the Centre de Recherche en Astrophysique du Quebec (CRAQ). B.A.L. is supported by the U.S. Department of Energy, Office of Science, under Award Number de-sc0013702 (Texas A&M University-Commerce) and the National Natural Science Foundation of China under Grant No. 11320101004.

-
- [1] G. S. Bisnovatyi-Kogan and V. M. Chechetkin, *Soviet Physics Uspekhi* **22**, 89 (1979).
- [2] K. Sato, *Progress of Theoretical Physics* **62**, 957 (1979).
- [3] P. Haensel and J. L. Zdunik, *Astron. & Astrophys.* **227**, 431 (1990).
- [4] P. Haensel and J. L. Zdunik, *Astron. & Astrophys.* **404**, L33 (2003).
- [5] P. Haensel and J. L. Zdunik, *Astron. Astrophys.* **480**, 459 (2008).
- [6] G. Ushomirsky and R. E. Rutledge, *Mon. Not. Roy. Astron. Soc.* **325**, 1157 (2001).
- [7] R. E. Rutledge, L. Bildsten, E. F. Brown, G. G. Pavlov, V. E. Zavlin, and G. Ushomirsky, *Astrophys. J.* **580**, 413 (2002).
- [8] P. S. Shternin, D. G. Yakovlev, P. Haensel, and A. Y. Potekhin, *Mon. Not. Roy. Astron. Soc.* **382**, L43 (2007).
- [9] E. F. Brown and A. Cumming, *Astrophys. J.* **698**, 1020 (2009).
- [10] A. Cumming, J. Macbeth, J. J. M. in 't Zand, and D. Page, *Astrophys. J.* **646**, 429 (2006).
- [11] A. Deibel, A. Cumming, E. F. Brown, and D. Page, *Astrophys. J.* **809**, L31 (2015).
- [12] L. Bildsten, E. E. Salpeter, and I. Wasserman, *Astrophys. J.* **384**, 143 (1992).
- [13] K. Scholberg, *Phys. Rev.* **D73**, 033005 (2006).
- [14] C. Amsler *et al.* (Particle Data Group), *Phys. Lett.* **B667**, 1 (2008).
- [15] S. Tavernier, "Experimental techniques in nuclear and particle physics," (Springer-Verlag Berlin Heidelberg, 2010).
- [16] C. J. Horowitz, *Phys. Rev.* **D65**, 043001 (2002).
- [17] C. J. Horowitz, K. J. Coakley, and D. N. McKinsey, *Phys. Rev.* **D68**, 023005 (2003).
- [18] J. N. Bahcall, *Phys. Rev.* **136**, B1164 (1964).
- [19] K. Langanke, G. Martinez-Pinedo, P. von Neumann-Cosel, and A. Richter, *Phys. Rev. Lett.* **93**, 202501 (2004).
- [20] P. Haensel, J. L. Zdunik, and J. Dobaczewski, *Astron. Astrophys.* **222**, 353 (1989).
- [21] D. G. Ravenhall, C. J. Pethick, and J. R. Wilson, *Phys. Rev. Lett.* **50**, 2066 (1983).
- [22] M. Hashimoto, H. Seki, and M. Yamada, *Prog. Theor. Phys.* **71**, 320 (1984).
- [23] C. P. Lorenz, D. G. Ravenhall, and C. J. Pethick, *Phys. Rev. Lett.* **70**, 379 (1993).
- [24] J. W. Negele and D. Vautherin, *Nucl. Phys.* **A207**, 298 (1973).
- [25] W.-C. Chen and J. Piekarewicz, *Phys. Rev.* **C90**, 044305 (2014).
- [26] P. B. Demorest, T. Pennucci, S. M. Ransom, M. S. E. Roberts, and J. W. T. Hessels, *Nature* **467**, 1081 (2010).
- [27] J. Antoniadis *et al.*, *Science* **340**, 6131 (2013).
- [28] E. Fonseca *et al.*, *Astrophys. J.* **832**, 167 (2016).
- [29] C. J. Horowitz and J. Piekarewicz, *Phys. Rev. Lett.* **86**, 5647 (2001).
- [30] F. Fattoyev, W. Newton, J. Xu, and B.-A. Li, *Phys. Rev.* **C86**, 025804 (2012).
- [31] K. Hebeler, J. Lattimer, C. Pethick, and A. Schwenk, *Phys. Rev. Lett.* **105**, 161102 (2010).
- [32] J. Casares, P. G. Jonker, and G. Israelian, arXiv:1701.07450.
- [33] P. Chang, L. Bildsten, and P. Arras, *Astrophys. J.* **723**, 719 (2010).
- [34] J. J. M. in 't Zand, A. Cumming, M. V. van der Sluys, F. Verbunt, and O. R. Pols, *Astron. Astrophys.* **441**, 675 (2005).
- [35] J. F. Crawford *et al.*, *Phys. Rev.* **C22**, 1184 (1980).
- [36] D. R. F. Cochran, P. N. Dean, P. A. M. Gram, E. A. Knapp, E. R. Martin, D. E. Nagle, R. B. Perkins, W. J. Shlaer, H. A. Thiessen, and E. D. Theriot, *Phys. Rev.* **D6**, 3085 (1972), [Erratum: *Phys. Rev.* D9,835(1974)].
- [37] P. Denes, B. D. Dieterle, D. M. Wolfe, T. Bowles, T. Dombek, J. E. Simmons, T. S. Bhatia, G. Glass, and W. B. Tippens, *Phys. Rev.* **C27**, 1339 (1983).
- [38] M. C. Lemaire *et al.*, in *19th International Workshop on Gross Properties of Nuclei and Nuclear Excitations Hirschegg, Austria, January 21-26, 1991* (1991) pp. 73–81.
- [39] R. L. Burman, M. E. Potter, and E. S. Smith, *Nucl. Instrum. Meth.* **A291**, 621 (1990).
- [40] W. W. Daehnick *et al.*, *Phys. Rev. Lett.* **74**, 2913 (1995).
- [41] J. G. Hardie *et al.*, *Phys. Rev.* **C56**, 20 (1997).
- [42] R. W. Flammang *et al.*, *Phys. Rev.* **C58**, 916 (1998).
- [43] P. Schwaller, M. Pepin, B. Favier, C. Richard-Serre, D. F. Measday, and P. U. Renberg, *Nucl. Phys.* **A316**, 317 (1979).
- [44] M. B. Tsang *et al.* (SPRIT), *Phys. Rev.* **C95**, 044614 (2017).
- [45] G. F. Bertsch, *Phys. Rev.* **C15**, 713 (1977).
- [46] M. Sandel, J. P. Vary, and S. I. A. Garpman, *Phys. Rev.* **C20**, 744 (1979).
- [47] J. Miller *et al.*, *Phys. Lett.* **B314**, 7 (1993).
- [48] L. Bildsten, E. E. Salpeter, and I. Wasserman, *Astrophys. J.* **408**, 615 (1993).
- [49] B.-A. Li, *Phys. Rev. Lett.* **88**, 192701 (2002).
- [50] B.-A. Li, *Nucl. Phys.* **A708**, 365 (2002).
- [51] B.-A. Li, *Phys. Rev.* **C92**, 034603 (2015).
- [52] K. S. Thorne, *Astrophys. J.* **212**, 825 (1977).
- [53] E. F. Brown, L. Bildsten, and R. E. Rutledge, *Astrophys. J.* **504**, L95 (1998).
- [54] E. M. Cackett, R. Wijnands, J. M. Miller, E. F. Brown, and N. Degenaar, *Astrophys. J.* **687**, L87 (2008).
- [55] D. Page and S. Reddy, (2012), arXiv:1201.5602 [nucl-th].
- [56] E. F. Brown, "dStar: Neutron star thermal evolution code," Astrophysics Source Code Library (2015), ascl:1505.034.

- [57] A. Deibel, A. Cumming, E. F. Brown, and S. Reddy, *Astrophys. J.* **839**, 95 (2017).
- [58] E. F. Brown, A. Cumming, F. J. Fattoyev, C. J. Horowitz, D. Page, and S. Reddy, *Phys. Rev. Lett.* **120**, 182701 (2018).
- [59] A. Cumming, E. F. Brown, F. J. Fattoyev, C. J. Horowitz, D. Page, and S. Reddy, *Phys. Rev.* **C95**, 025806 (2017).
- [60] C. J. Horowitz, D. K. Berry, C. M. Briggs, M. E. Caplan, A. Cumming, and A. S. Schneider, *Phys. Rev. Lett.* **114**, 031102 (2015).
- [61] A. Schwenk, B. Friman, and G. E. Brown, *Nucl. Phys.* **A713**, 191 (2003).
- [62] S. Gandolfi, A. Y. Illarionov, S. Fantoni, F. Pederiva, and K. E. Schmidt, *Phys. Rev. Lett.* **101**, 132501 (2008).
- [63] E. M. Cackett, E. F. Brown, A. Cumming, N. Degenaar, J. K. Fridriksson, J. Homan, J. M. Miller, and R. Wijnands, *Astrophys. J.* **774**, 131 (2013).
- [64] R. Wijnands, M. Nowak, J. M. Miller, J. Homan, S. Wachter, and W. H. G. Lewin, *Astrophys. J.* **594**, 952 (2003).
- [65] R. Wijnands, J. Homan, J. M. Miller, and W. H. G. Lewin, *Astrophys. J. Lett.* **606**, L61 (2004).
- [66] H. Negoro, K. Furuya, S. Ueno, H. Tomida, S. Nakahira, M. Kimura, M. Ishikawa, Y. E. Nakagawa, T. Mihara, M. Sugizaki, M. Serino, M. Shidatsu, J. Sugimoto, T. Takagi, M. Matsuoka, N. Kawai, Y. Tachibana, T. Yoshii, A. Yoshida, T. Sakamoto, Y. Kawakubo, H. Ohtsuki, H. Tsunemi, R. Imatani, M. Nakajima, T. Masumitsu, K. Tanaka, Y. Ueda, T. Kawamuro, T. Hori, Y. Tsuboi, S. Kanetou, M. Yamauchi, D. Itoh, K. Yamaoka, and M. Morii, *The Astronomer's Telegram* **7943**, 1 (2015).
- [67] Y. B. Zel'dovich and N. I. Shakura, *Soviet Astronomy* **13**, 175 (1969).
- [68] S. L. Shapiro and E. E. Salpeter, *Astrophys. J.* **198**, 671 (1975).
- [69] L. Bildsten, P. Chang, and F. Paerels, *Astrophys. J.* **591**, L29 (2003).